Interplay between interferences and electron-electron interactions in epitaxial graphene

B. Jouault,[1,2] B. Jabakhanji,[1] N. Camara,[1,3] W. Desrat,[1] C. Consejo,[1] and J. Camassel[1,2]

[1]*Université Montpellier 2, Laboratoire Charles Coulomb, cc074, place Eugène Bataillon, F-34095 Montpellier cedex 5, France*

[2]*CNRS, UMR 5650, cc074, place Eugène Bataillon, F-34095 Montpellier cedex 5, France*

[3]*CNM, Campus UAB, Bellaterra (Barcelona), Spain*

(Received 2 December 2010; published 9 May 2011)

We separate localization and interaction effects in epitaxial graphene devices grown on the C face of an 8°-off-axis 4*H*-SiC substrate by analyzing the low-temperature conductivities. Weak localization and antilocalization are extracted at low magnetic fields, after elimination of a geometric magnetoresistance and subtraction of the magnetic-field-dependent Drude conductivity. The electron-electron interaction correction is extracted at higher magnetic fields, where localization effects disappear. Both phenomena are weak but sizable and of the same order of magnitude. If compared to graphene on silicon dioxide, the electron-electron interactions on epitaxial graphene are not significantly reduced by the larger dielectric constant of the SiC substrate.

DOI: 10.1103/PhysRevB.83.195417 PACS number(s): 72.80.Vp, 73.20.Fz

I. INTRODUCTION

Graphene-based devices are exciting candidates for future generations of microelectronic devices. A promising technique to produce graphene at an industrial scale is epitaxial graphene growth from a SiC substrate, because these SiC substrates can be patterned using standard lithography methods. Thanks to recent technical improvements, the most delicate and intrinsic features of graphene, those reflecting the chiral nature of the quasiparticles, such as, for instance, the so-called half-integer quantum Hall effect[1–4] and the weak antilocalization,[5] have been recently reported for epitaxial graphene.

In graphene, depending on the relative magnitude of the intervalley scattering time and phase coherence time, either weak localization (WL) or weak antilocalization (WAL) has been predicted.[6] The phase interference correction to the resistance depends on the nature of the disorder. For epitaxial graphene samples, elastic scattering favorable for WAL can be caused by remote charges like ionized impurities in the substrate. On the other hand, atomically sharp disorder (local defects, edges) causes intervalley scattering and gives rise to WL.

Experimentally, in two-dimensional gases, WL is often mixed with the electron-electron interaction[7] (EEI). Like WL, EEI gives a correction to the Drude conductivity with a $\ln T$ dependence. It follows that the experimental extraction and separation of EEI, WL, and WAL contribution are usually difficult.[8] For graphene, in the diffusive regime, EEI is expected to give this usual temperature-dependence correction proportional to $\ln(T)$. EEI is also expected to be sensitive to the different kinds of disorder.[9]

In this work, we take advantage of simultaneous measurements of the longitudinal and transverse resistances to invert the resistivity tensor. We can then separate the different mechanisms which give corrections to the Drude conductivity: (i) a geometric contribution, which experimentally appears as a constant term in the longitudinal conductivity; (ii) WL and WAL, by a comparison between the experimental magnetoconductance and the Drude magnetoconductivity; (iii) EEI, whose temperature dependence can be analyzed in the magnetic field range for which WAL has disappeared.

II. EXPERIMENTAL DETAILS

We have used large and homogeneous single epitaxial graphene layers grown on the C face of an insulating 8° off-axis 4*H*-SiC substrate. The graphene sheets have an elongated triangular shape whose quality and homogeneity can be easily checked using micro-Raman spectroscopy. On a few selected samples, Cr/Au Ohmic contacts were deposited to define Hall bars with a rough geometry (see inset in Fig. 1 for details). Then magnetotransport measurements were done using a 14 T magnet in a cryostat and a variable temperature inset operated down to 1.5 K. On the best samples, at high magnetic field, the half-integer quantum Hall effect could be observed up to the last plateau in the temperature range 1.5 to 40 K. For details, see Ref. 10. In this work we focus on two moderately doped samples ($S1$ and $S2$) with dimensions, carrier concentration, mobility, and scattering times reported in Table I. We work at low injection currents (10 nA–1 μA), mainly at low magnetic fields ($|B| \leqslant 3$ T) and low temperatures (1.5–200 K), and we focus on the magnetic field dependence of the longitudinal and transverse elements of the resistivity tensor.

III. BACKGROUND CONSIDERATIONS

An overview of the results obtained for sample $S1$ is shown in Fig. 1. The experimental longitudinal and transverse magnetoresistances $R_{xx}(B)$ and $R_{xy}(B)$ for sample $S1$ are presented in Figs. 1(a) and 1(b), respectively, at different temperatures between 1.6 and 48 K. Let us consider first Fig. 1(a). At low fields ($B \leqslant 0.1$ T), a negative magnetoresistance peak centered at $B = 0$ T is observed in R_{xx}. This peak is typical of weak localization. Indeed, this peak shows a linear dependence of R_{xx} vs $\ln(T)$ with a slope of the order of h/e^2 [see inset of Fig. 1(a)] and the amplitude of the peak is $\Delta\rho_{xx} \approx 2\rho_{xx}^2 e^2/h$ (ρ_{xx} is the longitudinal resistivity). At higher magnetic fields, reproducible fluctuations in the conductance G are also observed, with amplitudes $\Delta G \approx 0.5e^2/h$ for $S1$ and $\Delta G \approx 0.1e^2/h$ for $S2$. Besides, the increase of the resistivity above 50 K [inset of Fig. 1(a)] is not strictly linear in T, which suggests that both phonons and impurities contribute to the temperature dependence.[11]

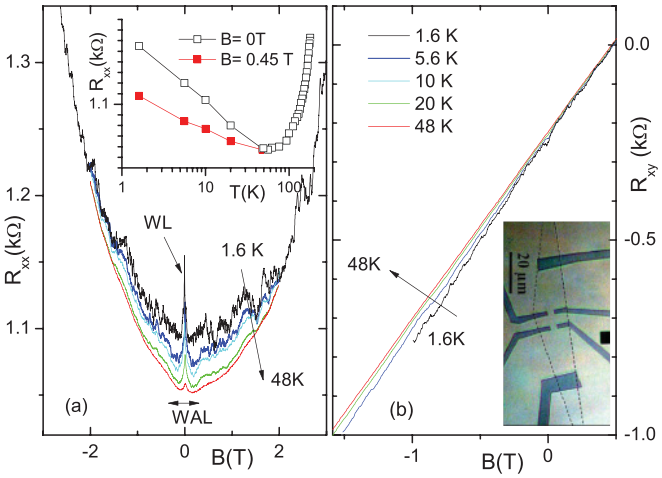

FIG. 1. (Color online) (a) $R_{xx}(B)$ at different temperatures for sample $S1$. All curves cross at $B \approx 2$ T and have a B^2 behavior. Inset shows the temperature dependence of R_{xx} at $B = 0$ (black open squares) and 0.45 T (solid red squares). (b) $R_{xy}(B)$ at different temperatures. The slope of the Hall voltage increases when T decreases due to electron-electron interactions. Inset: Photograph of sample $S1$; the edges of the graphene layer have been indicated by a dashed line.

At low temperatures ($\leqslant$50 K) and at magnetic fields $|B| \leqslant 0.4$ T, a smooth depression is observed in R_{xx}, which we attribute to weak antilocalization. Because this WAL is barely visible in Fig. 1(a), we also present additional experimental results in Appendix A. Experimentally, WAL is blurred because fluctuations of conductance are also present, and also because the positive magnetoresistance of the WAL is superposed on another positive magnetoresistance with a pronounced parabolic dependence, which is well observed in the whole magnetic field range $|B| \leqslant 3$ T presented in Fig. 1(a). The theory of weak localization is based on the diffusion approximation and does not hold for magnetic fields much higher than $B_{tr} = \hbar/4eD\tau_{tr} \approx 100$ mT, where D is the diffusion coefficient and τ_{tr} the transport time. This means that no part of the parabolic background above B_{tr} can be due to WL features. It must have a different origin. Since the device is far from having the shape of an ideal Hall bar [see inset in Fig. 1(b)] we ascribe this parabolic magnetoresistance component to magnetic deflection of the current lines. This is because the lateral probes are invasive and because the graphene layer under the lateral contacts is likely to have different mobility and carrier concentration.[12] For details, see Appendix B.

Beyond geometric and interference corrections, a third correction to the resistivity manifests. It comes from electron-electron interactions and shows as (i) the persistence of a $\ln(T)$ linear temperature dependence of R_{xx}, in a magnetic field range where interference effects are suppressed [see inset of Fig. 1(a) for a field of $B = 0.45$ T]; (ii) a variation of the Hall slope [Fig. 1(b)] as a function of T, which cannot be explained by variations of the carrier density, as the hole gas is strongly degenerate ($E_F/k_BT \geqslant 20$ for $T \leqslant 50$ K, where E_F is the Fermi energy); (iii) a crossing of all $R_{xx}(B)$ resistances taken at different temperatures at $B \approx 1/\mu$ [Fig. 1(a)].[13]

TABLE I. Properties of samples $S1$ and $S2$: length L between lateral probes, width W (in μm), hole concentration (in 10^{12} cm^{-2}), mobility (in cm^2 V^{-1} s^{-1}), scattering times τ_{sr}, τ_{lr}, and τ_{tr} (in ps) and diffusion constant (in m^2 s^{-1}).

Sample	L	W	n_s	μ	τ_{sr}	τ_{lr}	τ_{tr}	D
$S1$	5	5	1.1	5000	0.57	0.1	0.065	0.03
$S2$	40	10	0.8	11000	0.48	0.15	0.11	0.057

The justification of the last two points, originally given in Ref. 13, is as follows. EEIs give no correction to the transverse conductance σ_{xy}. This result, which implies that the conductivity correction cannot be interpreted as a conventional density-of-states correction, was first demonstrated in Ref. 7. Details of the calculation can be found in Ref. 14. By contrast, EEI gives a small correction $\delta\sigma^{ee}$ to the longitudinal conductance σ_{xx}. This correction does not depend on B if the magnetic field is smaller than a critical field $B_S \leqslant \pi k_B T/2\mu_B$. This condition is fulfilled for all the temperature and magnetic field ranges of this study. Because of this correction, the EEI gives rise to a negative magnetoresistance in the first order in $\delta\sigma^{ee} \ll \sigma_{xx}$:

$$\rho_{xx} \sim 1/\sigma_0 - (1 - \mu^2 B^2)\delta\sigma^{ee}/\sigma_0^2, \tag{1}$$

and a variation of the Hall slope $\delta\rho_{xy}/\rho_{xy} \approx -2\delta\sigma^{ee}/\sigma_0$ where σ_0 is the conductivity at $B = 0$. These relations are derived by inverting the conductivity tensor:

$$\rho_{xx} = \frac{\sigma_{xx}}{\sigma_{xx}^2 + \sigma_{xy}^2}, \tag{2}$$

$$\rho_{xy} = \frac{\sigma_{xy}}{\sigma_{xx}^2 + \sigma_{xy}^2}. \tag{3}$$

It has been established recently[8] that the separation of EEI and WL is simplified if the magnetoconductivities $\sigma_{xy}(B)$ and $\sigma_{xx}(B)$ are used, rather than the resistivities. As already stressed, the conductivity of the graphene layer is different below the Cr/Au contacts and, strictly speaking, inverting the resistivity tensor is incorrect because the device is inhomogeneous. However, experimentally, the geometric correction is small and appears only in the longitudinal magnetoresistance as a parabolic correction, and consequently geometric corrections to the longitudinal conductivity appear as a B-independent shift $\delta\sigma^G$.

The magnetoconductivities for sample $S1$ are plotted in Fig. 2 at different temperatures. The conductivities have been obtained from Eqs. (2) and (3), where the resistivities have been estimated from $\rho_{xx} \approx (W/L)[R_{xx}(B) + R_{xx}(-B)]/2$ and $\rho_{xy} \approx [R_{xy}(B) - R_{xy}(-B)]/2$. The lower inset of Fig. 2 shows that all $\sigma_{xy}(B)$ taken at different temperatures collapse on the same curve, as expected for EEIs. This also confirms that both mobility and carrier concentration are constant over the whole temperature range and, as the geometric correction only depends on T via the Hall angle μB, that $\delta\sigma^G$ does not depend on the temperature. Finally, the T independence of the transverse conductivity indicates an effective separation of EEI ($\delta\sigma^{ee}$) and interference ($\delta\sigma^{wl}$) corrections over almost the whole B range. At low fields $|B| \leqslant B_{tr}$, a T dependence of σ_{xy} due to WL is expected but is not observed, being beyond our experimental resolution.

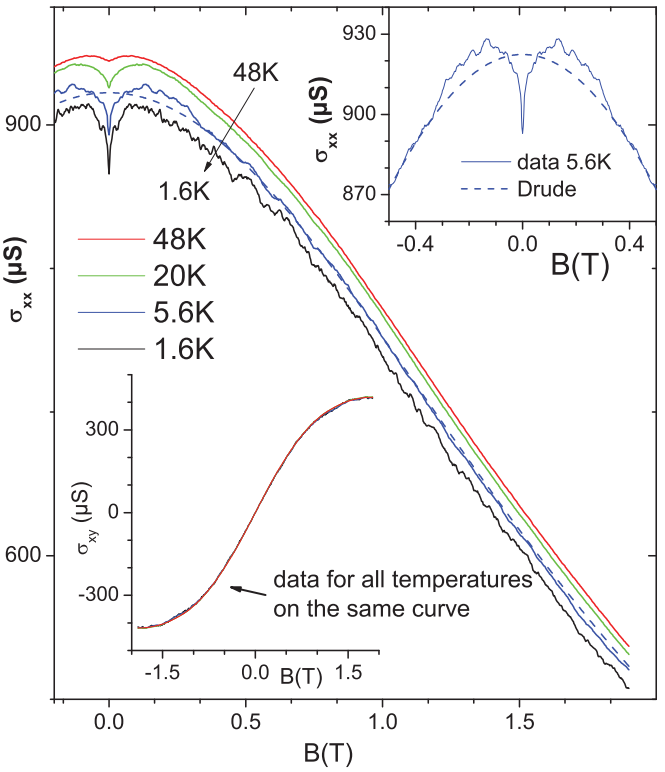

FIG. 2. (Color online) Longitudinal conductivity σ_{xx} versus B at different temperatures for sample $S1$. Blue dashed line is the best fit of the conductivity at $T = 5.6$ K, on a B interval 0.5–2 T. The fit is done according to $\sigma_{xx}^{D}(B) + C$ (see text). The upper inset is the enlargement of the area around $B \sim 0$ T. The lower inset shows that all transverse conductivities $\sigma_{xy}(B)$, taken at different temperatures, collapse on a single curve.

The large decrease of $\sigma_{xx}(B)$ between 0 and 2 T in Fig. 2 is due to the magnetic field dependence of the Drude conductivity $\sigma^D = \sigma_0/(1 + \mu^2 B^2)$. We express the total conductivity by

$$\sigma_{xx} = \sigma^D + \delta\sigma^{ee} + \delta\sigma^G + \delta\sigma^{wl}. \quad (4)$$

When WL is negligible, $|B| \geqslant 0.5 \gg B_{tr}$, we impose $\delta\sigma^{wl} = 0$ and Eq. (4), for a given temperature, simplifies to $\sigma_{xx} = \sigma^D + C$, where C is a constant which incorporates both geometric and EEI corrections. This last formula gives very good fits to the conductivity at all temperatures. As an example, the blue dotted line in Fig. 2 is the fit for the $T = 5.6$ K data in the interval 0.5–2 T, where σ_0, μ, and C are the fit parameters. Transverse and longitudinal resistivities can be fitted separately but still give very similar mobilities and concentrations, which are reported in Table I.

The upper inset in Fig. 2 is an enlargement of the low-B data at $T = 5.6$ K and evidences the weak antilocalization peak which occurs around the weak localization centered at $B = 0$. A similar weak antilocalization can be detected for all temperatures. The WL theory does not take into account the modification of the current paths due to the magnetic field. In other words, before examining the WL contribution to the conductivity, we should first subtract the Drude fits $\sigma^D + C$ (given by the dotted line in Fig. 2) to the observed longitudinal conductivities.[15] Experimental results for samples $S2$ and $S1$ are shown in Fig. 3, for different temperatures.

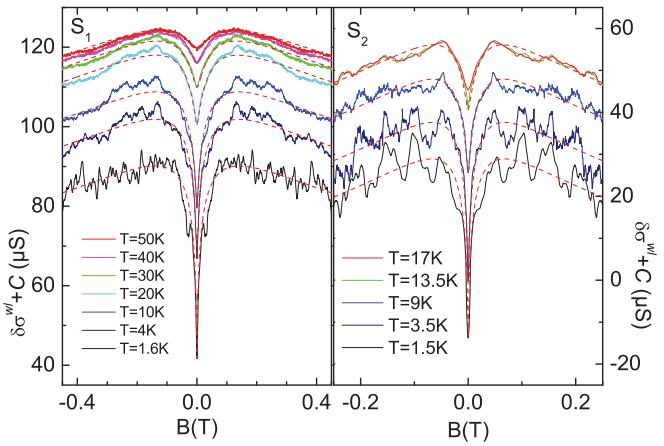

FIG. 3. (Color online) (a) Corrections to the conductivities $\delta\sigma^{wl} + C$ at different temperatures for sample $S1$. The T-dependent vertical shift C has been kept for clarity. WL fits according to Eq. (5) are also indicated. (b) Similar analysis for sample $S2$.

IV. CORRECTION DUE TO WEAK LOCALIZATION AND ANTILOCALIZATION

In the diffusive regime in graphene, $\delta\sigma^{wl}$ is given by[6]

$$\delta\sigma^{wl} = \frac{e^2}{\pi h}\left[F\left(\frac{B}{B_\varphi}\right) - F\left(\frac{B}{B_\varphi + 2B_{sr}}\right) - 2F\left(\frac{B}{B_\varphi + B_{sr} + B_{lr}}\right)\right], \quad (5)$$

where $F(z) = \ln z + \Psi(1/2 + 1/z)$, Ψ is the digamma function, $B_{\varphi,sr,lr} = \hbar/4De\tau_{\varphi,sr,lr}$, and $\tau_{\varphi,sr,lr}$ are the coherence time, the intervalley scattering time, and the intravalley scattering time respectively. For simplicity, we identify intervalley as short range (sr) scattering and intravalley as long-range (lr) scattering. We take constant scattering times τ_{sr} and τ_{lr} over the whole temperature range and only τ_φ is allowed to depend on T. Neglecting the warping,[16] we also impose $\tau_{tr}^{-1} = \tau_{sr}^{-1} + \tau_{lr}^{-1}$. We then fit the conductivities at different temperatures by Eq. (5). Results are indicated by dashed lines in Fig. 3 (for the sake of clarity, fits at high temperatures have not been reported). The best fit is obtained with the values reported in Table I. We estimate the short-range scattering length $L^{sr} = \sqrt{D\tau^{sr}} \approx$ 100–140 nm. The long-range scattering length $L^{lr} = \sqrt{D\tau^{lr}} \approx$ 70–90 nm is even shorter. These lengths are comparable to what is found in exfoliated graphene on a SiO_2 substrate.[17] They are also comparable to the distance between the SiC steps below the graphene layer. It is often stated that exfoliated graphene is much more disordered at the edge of the SiC steps.[18] Therefore step edges could be the main source of scattering in these samples.

The phase coherence time τ_φ obtained from the fit is plotted in Fig. 4. Apart from a saturation at low T, τ_φ is roughly proportional to $1/T$ between 10 and 50 K with a slope equal to ≈50 ps K for samples $S1$ and $S2$. We conclude that τ_φ obeys the usual temperature dependence for electron-electron scattering in the diffusive regime:

$$\tau_\varphi^{-1} = \beta k_B T \ln g/\hbar g, \quad (6)$$

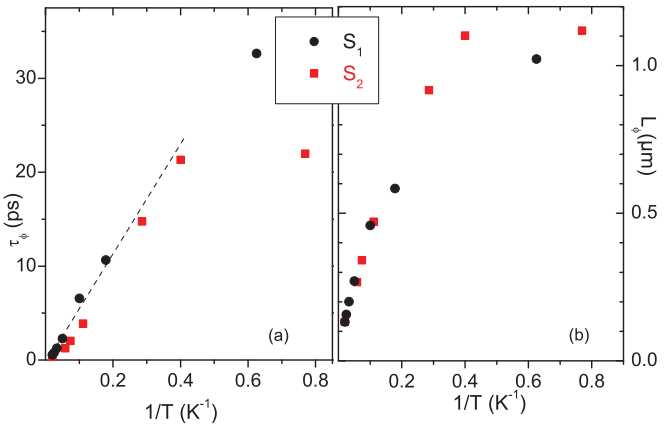

FIG. 4. (Color online) (a) Phase coherence time τ_φ extracted from the fit of the WL; see Fig. 3. Black circles, sample $S1$; red squares, sample $S2$. τ_φ is roughly proportional to $1/T$ between 60 and 2.5 K and saturates at lower temperatures. The dashed line is a guide for the eyes. (b) Coherence length L_φ versus $1/T$, for the two samples.

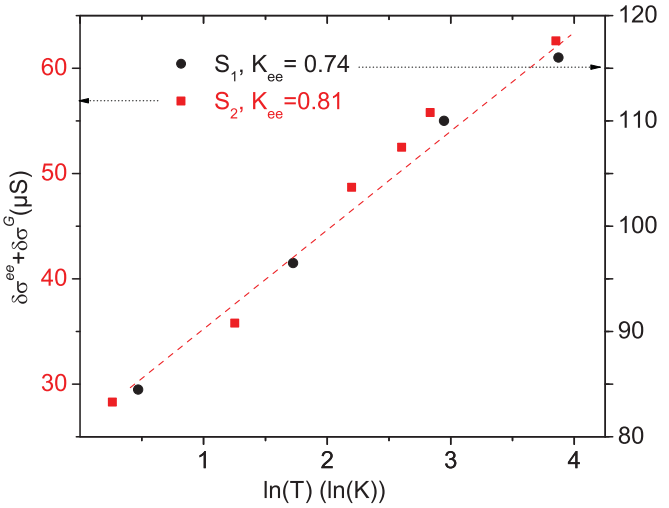

FIG. 5. (Color online) Experimental temperature dependence of $C(T) = \delta\sigma^G + \delta\sigma^{ee}(T)$ vs $\ln(T)$ for samples S1 and S2. The slope gives $K_{ee} = 0.81$ and 0.74 for S2 and S1, respectively.

where g is the reduced conductivity, $g = \sigma_0 h/e^2$, and the empirical coefficient β is 1 for $S1$ and 1.4 for $S2$. Similar observations have already been made for both epitaxial[5] and exfoliated graphene.[17,19] The coherence length $L_\varphi = \sqrt{D\tau_\varphi}$ is readily calculated and plotted in Fig. 4(b). At low temperature, L_φ slightly exceeds 1 μm.

V. CORRECTION DUE TO ELECTRON-ELECTRON INTERACTION

We attribute the temperature dependence of the conductivity to EEI. The Drude mobility is constant over the whole temperature range; therefore there is no temperature dependence of the conductivity induced by electron-phonon scattering. This is not surprising, as the temperature dependence for graphene is small below the Grüneisen temperature T_{BG} given by $T_{BG} \approx 54\sqrt{n_s}$ K, where the concentration n_s is in units of 10^{12} cm^{-2}.[11,20] For our samples, $T_{BG} \approx 54$ K, and almost all our measurements are done below the Grüneisen temperature.

As $k_B T \tau_{tr}/\hbar \ll 1$, we are by definition in the diffusive regime, for which EEI theory predicts a temperature-dependent correction to the conductivity given by

$$\delta\sigma^{ee} = K_{ee}\frac{e^2}{\pi h}\ln\frac{k_B T\tau_{tr}}{\hbar}, \tag{7}$$

where K_{ee} is a prefactor whose value depends on the different channels contributing to the EEIs.[9] In Fig. 5, we show $\delta\sigma_{xx}(T)$ for samples $S2$ and $S1$. Consistency with Eq. (7) implies that $\delta\sigma^{ee}$, which is only a part of $\delta\sigma_{xx}(T)$, is negative over the whole temperature range presented in Fig. 5. The expected $\ln(T)$ dependence is evidenced and the slope gives $K_{ee} = 0.81 \pm 0.05$ and 0.74 ± 0.07 for samples $S2$ and $S1$, respectively. These values are very similar to recent experimental findings on exfoliated graphene.[9,21] In a two-dimensional (2D) system with a single valley, K_{ee} takes the form[22]

$$K_{ee} = 1 + c\left[1 - \ln(1 + F_0^\sigma)/F_0^\sigma\right], \tag{8}$$

where the unity represents the so-called charge contribution (the Fock and singlet part of the Hartree term), the c prefactor is the number of "triplet" channels (from the Hartree term), and F_0^σ is the liquid Fermi constant. At low temperatures ($k_B T \leqslant \hbar/\tau_{sr}$) ($T \leqslant 15$ K for $S2$ and 30 K for $S1$), when long-

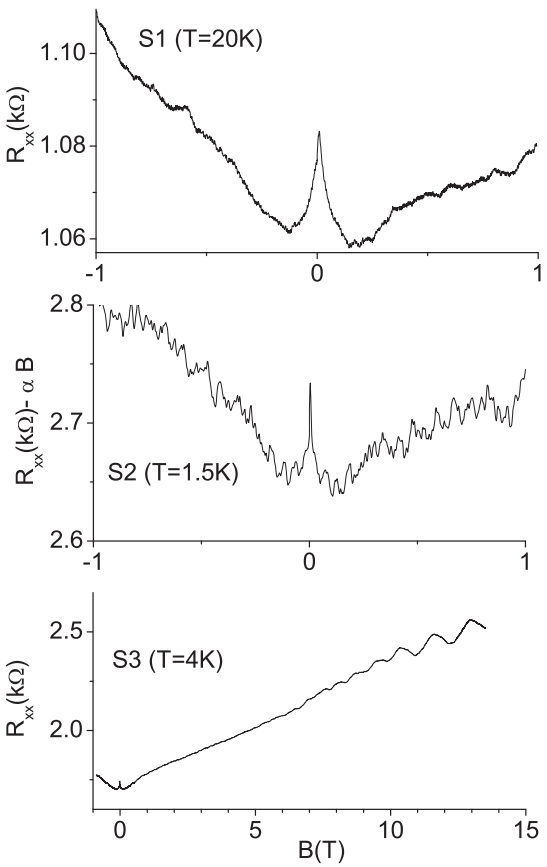

FIG. 6. Transverse magnetoresistance for three different samples. A small depression attributed to WAL is visible around the WL peak for all three samples.

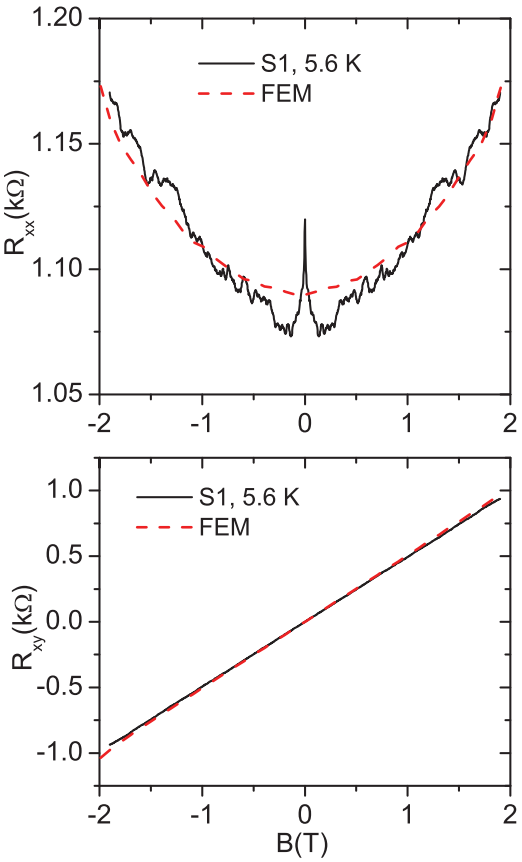

FIG. 7. (Color online) Experimental longitudinal and transverse magnetoresistances (only the symmetric or antisymmetric parts have been kept for clarity) for sample $S1$ compared to the result of a numerical model based on the FEM. The model imposes an increased hole concentration ($n_s = 7 \times 10^{12}$ cm^{-2}) and a reduced mobility ($\mu = 0.06$ m^2 V^{-1} s^{-1}) under the lateral probes. The rest of the graphene layer keeps its parameters as defined in Table I.

and short-range scattering rates are important, the usual single-valley case is recovered with a prefactor $c = 3$. This leads to $F_0^\sigma = -0.13 \pm 0.04$. This value is small and very close to the value of F_0^σ recently found for exfoliated graphene.[9] This is somewhat surprising, as the dielectric constant in SiC (10) is larger than that in SiO_2 (3.9) and we would expect even smaller electron-electron interactions because of the screening of the substrate. However, numerical estimation of F_0^σ following, for instance, Ref. 9 gives $F_0^\sigma \approx -0.09$: a value compatible with our experiment. Also, Ref. 23 predicts values for the Fermi liquid constant only slightly smaller than our findings. Interestingly, it was also recently quoted[9] that at intermediate temperatures $\hbar/\tau_{sr} \leqslant k_B T \leqslant \hbar/\tau_{lr}$, additional triplet channels originating from pseudospin conservation (i.e., valley degeneracy) become relevant, and the number of triplet channels increases to $c = 7$. However, we do not observe any change in the slope in Fig. 5 from $T = 1.5$ up to 50 K. The situation is similar in Ref. 21, where EEI is observed in a temperature range for which the slope should vary, but where experimentally the slope remains constant.

To conclude, we show, beyond classical geometric corrections, weak localization, weak antilocalization, and electron-electron interactions in epitaxial graphene. Weak antilocalization is observable directly in the resistances, and its analysis gives access to the different scattering times, which are very close to those for exfoliated graphene on SiO_2 substrates. Electron-electron interaction also gives a small correction to the conductivity, which is not significantly smaller than in exfoliated graphene.

ACKNOWLEDGMENTS

We acknowledge the EC for partial support through the RTN ManSiC Project, the French ANR for partial support through the Project Blanc GraphSiC, and the Spanish Government for a Juan de la Cierva grant . N.C. also acknowledges A. Bachtold, A. Barreiro, and J. Moser from ICN Barcelona, for technical and theoretical supports.

APPENDIX A

In Fig. 6, we present the magnetoresistances of samples $S1$ and $S2$ and of an additional monolayer $S3$, more highly doped. A straight line αB has been subtracted for sample $S2$, for clarity. For all three samples, a dip is observed on the two sides of the central WL peak. We attribute the dip to WAL.

APPENDIX B

We suggest that most of the parasitic magnetoresistance comes from the invasive lateral probes. In order to sustain this assumption, classical magnetoresistances can be calculated by means of the finite element method (FEM) for the geometry of the devices. The simplest model only assumes different concentration and mobility under the lateral probes, and the results of this model are shown in Fig. 7 for sample $S1$. There is good agreement with the experiment for a reduced mobility and an increased concentration under the probes, which seems reasonable if these regions have been damaged during the electron beam lithography.

[1] T. Shen, J. J. Gu, M. Xu, Y. Q. Wu, M. L. Bolen, M. A. Capano, L. W. Engel, and P. D. Ye, Appl. Phys. Lett. **95**, 172105 (2009).
[2] J. Jobst, D. Waldmann, F. Speck, R. Hirner, D. K. Maude, T. Seyller, and H. B. Weber, Phys. Rev. B **81**, 195434 (2010).
[3] A. Tzalenchuk, S. Lara-Avila, A. Kalaboukhov, S. Paolillo, M. Syvajarvi, R. Yakimova, O. Kazakova, T. J. B. M. Janssen, V. Fal'ko, and S. Kubatkin, Nature Nano. **5**, 186 (2010).
[4] X. Wu, Y. Hu, M. Ruan, N. K. Madiomanana, J. Hankinson, M. Sprinkle, C. Berger, and W. A. de Heer, Appl. Phys. Lett. **95**, 223108 (2009).
[5] X. Wu, X. Li, Z. Song, C. Berger, and W. A. de Heer, Phys. Rev. Lett. **98**, 136801 (2007).
[6] K. Kechedzhi, E. McCann, H. Suzuura, and B. Altshuler, Eur. Phys. J. Spec. Top. **148**, 39 (2007).

[7]B. L. Altshuler, A. G. Aronov, and P. A. Lee, Phys. Rev. Lett. **44**, 1288 (1980).
[8]K. E. J. Goh, M. Y. Simmons, and A. R. Hamilton, Phys. Rev. B **77**, 235410 (2008).
[9]A. A. Kozikov, A. K. Savchenko, B. N. Narozhny, and A. V. Shytov, Phys. Rev. B **82**, 075424 (2010).
[10]N. Camara, B. Jouault, A. Caboni, B. Jabakhanji, W. Desrat, E. Pausas, C. Consejo, N. Mestres, P. Godignon, and J. Camassel, Appl. Phys. Lett. **97**, 093107 (2010).
[11]E. H. Hwang and S. Das Sarma, Phys. Rev. B **77**, 115449 (2008).
[12]B. Huard, N. Stander, J. A. Sulpizio, and D. Goldhaber-Gordon, Phys. Rev. B **78**, 121402 (2008).
[13]G. M. Minkov, O. E. Rut, A. V. Germanenko, A. A. Sherstobitov, V. I. Shashkin, O. I. Khrykin, and V. M. Daniltsev, Phys. Rev. B **64**, 235327 (2001).
[14]B. Altshuler and A. G. Aronov, *Electron-Electron Interactions in Disordered Systems* (Elsevier, Amsterdam, 1985), Chap. 1.
[15]Y. Y. Proskuryakov, A. K. Savchenko, S. S. Safonov, M. Pepper, M. Y. Simmons, and D. A. Ritchie, Phys. Rev. Lett. **86**, 4895 (2001).
[16]Y.-F. Chen, M.-H. Bae, C. Chialvo, T. Dirks, A. Bezryadin, and N. Mason, J. Phys.: Condens. Matter **22**, 205301 (2010).
[17]F. V. Tikhonenko, D. W. Horsell, R. V. Gorbachev, and A. K. Savchenko, Phys. Rev. Lett. **100**, 056802 (2008).
[18]B. Jouault, B. Jabakhanji, N. Camara, W. Desrat, A. Tiberj, J.-R. Huntzinger, C. Consejo, A. Caboni, P. Godignon, Y. Kopelevich *et al*., Phys. Rev. B **82**, 085438 (2010).
[19]S. V. Morozov, K. S. Novoselov, M. I. Katsnelson, F. Schedin, L. A. Ponomarenko, D. Jiang, and A. K. Geim, Phys. Rev. Lett. **97**, 016801 (2006).
[20]T. Stauber, N. M. R. Peres, and F. Guinea, Phys. Rev. B **76**, 205423 (2007).
[21]J. Moser, H. Tao, S. Roche, F. Alsina, C. M. Sotomayor Torres, and A. Bachtold, Phys. Rev. B **81**, 205445 (2010).
[22]N. N. Klimov, D. A. Knyazev, O. E. Omel'yanovskii, V. M. Pudalov, H. Kojima, and M. E. Gershenson, Phys. Rev. B **78**, 195308 (2008).
[23]M. Polini, R. Asgari, Y. Barlas, T. Pereg-Barnea, and A. MacDonald, Solid State Commun. **143**, 58 (2007).